SENSITIVITY ANALYSIS OF PARCELLATION IN THE JOINT DETECTION-ESTIMATION OF BRAIN ACTIVITY IN fMRI

Thomas Vincent[(1,2)]*, Philippe Ciuciu*[(1,2)] *and Bertrand Thirion*[(3)]

[(1)] CEA/NeuroSpin, Bâtiment 145, F-91191 Gif-sur-Yvette, cedex France
[(2)] IFR 49, Functional neuroimaging institute, Paris, France
[(3)] INRIA Saclay Parietal, NeuroSpin, Bât. 145, F-91191 Gif-sur-Yvette, cedex France
[1,3] firstname.lastname@cea.fr

ABSTRACT

Within-subject analysis in fMRI relies on both (i) a detection step to localize which parts of the brain are activated by a given stimulus type, and on (ii) an estimation step to recover the underlying brain dynamics. In [1], a Bayesian detection-estimation approach that jointly addresses (i)-(ii) has been proposed. In the latter, a functionally homogeneous parcellation of the brain is required prior to this analysis. If tools exist to produce suitable parcellations [2], the question remains open of its impact on both activation detection and dynamics estimation. Here, we present a sensitivity analysis of this Bayesian model regarding the parcellation. We show that some activating clusters are stable regarding parcellation while others are highly variable. The overall procedure is quite sensitive to the input parcellation as the uncertainty of the estimated effect is correlated to its size. The perspective is to extend our model with an adaptive parcellation combined with the detection-estimation.

Index Terms— sensitivity analysis, Bayes procedures, Magnetic resonance imaging.

1. INTRODUCTION

The overall aim of functional Magnetic Resonance Imaging (fMRI) is the understanding of the relation between functions (cognitive or sensori-motor) and anatomic structures in the human brain. In order to obtain results relevant to the population scale, the same fMRI experiment is repeated over a cohort of volunteers or patients. Each fMRI acquisition on one subject yields the variations of the blood oxygenation over a 4-dimensional lattice (3D in space, and time): the BOLD signal. The analysis of such group data is performed in two steps: results of separate within-subject analyses ("first level") are combined in a between-subject analysis ("second level"). Here, we are interested in the first level, fulfilling it by a joint detection-estimation (JDE) process [1]. The central assumption governing the Hemodynamic Response Function (HRF) estimation in this JDE is the shape invariance of the BOLD response when considering a small part of the brain. Indeed, the HRF is interpreted as a regional physiological response inherent to the vascular system spanning a region of interest and locally modulated only in magnitude by neural-induced activity at the voxel level. The optimal setting of the parcel number to correctly parcellate the brain has been adressed in [3]: around 400 to 500 parcels with sizes of few hundreds of voxels. Here, we are interested in the effect of position: if the local aspect prevails in the HRF estimation, then shifts in parcel positions would induce little variability in the results. At the opposite, observing strong variations would imply that there exist some local frontiers/edges where hemodynamics significantly change. In this case, we would confirm that the most *reliable* parcellation procedure is mandatory prior to the Bayesian region-based analysis, in order to clearly identify these regions.

This work was supported by grants from Région Ile-de-France.

2. PARCELLING THE BRAIN

Apart from serving the purpose of the Bayesian first level fMRI analysis presented here, brain parcellations are typically used to define Regions Of Interest (ROIs) in order to better understand the anatomical substrate of brain activity. For instance, anatomical parcellations that describe and cluster the cortical surface into gyri [4] can help to better define activated regions.

In another respect, a complete region-based approach comprising the first and second level analyses can be carried out as in [2]. Given the mis-registrations remaining even after spatial normalization, a given voxel in the common MNI space may not represent the same anatomo-functional structure across subjects. Grouping voxels into parcels provides the ability to correct part of the functional mis-correspondance.

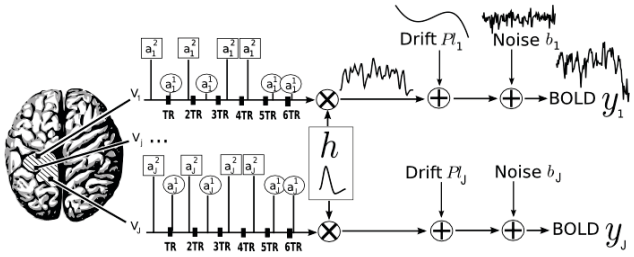

Fig. 1. Parcel-based model of the BOLD signal in the JDE framework. Forward BOLD signal generations are detailed for a single brain parcel (hatched area). Two different stimulus types are considered, represented by squares or circles surrounding the neural response levels a_j^m.

3. DETECTION-ESTIMATION PROCEDURE

Here, the parcel-based model of the BOLD signal introduced in [5] is adopted: a linear time-invariant (LTI) system. It characterizes every parcel $\mathcal{P} = (V_j)_{j=1:J}$ by a single HRF shape and accounts for voxel-dependent and stimulus-related fluctuations of the magnitude of the BOLD signal. The fMRI time course measured in voxel V_j at times $(t_n)_{n=1:N}$ (where $t_n = nTR$, N being the number of scans and TR, the time of repetition) then reads $\boldsymbol{y}_j = \sum_{m=1}^{M} a_j^m \boldsymbol{X}^m \boldsymbol{h} + \boldsymbol{P}\boldsymbol{\ell}_j + \boldsymbol{b}_j, \quad \forall\, j,\ V_j \in \mathcal{P}, m = 1:M$ stands for the condition index. This model remains time-invariant while it incorporates spatially-varying and stimulus-related magnitudes, called *Neural Response Levels* (NRLs) and denoted $\mathbb{a} = (\boldsymbol{a}_j^m)_{j=1:J,m=1:M}$ in the following. $\boldsymbol{X}^m = (x_{t_n - d\Delta t}^m)_{n=1:N,d=0:D}$ denotes the $N \times (D+1)$ binary matrix that codes the arrival times of the mth stimulus which are approximated to fit a Δt-sampled grid, where Δt is the sampling period of the HRF ($\Delta t < TR$). Vector $\boldsymbol{h} = (h_{d\Delta t})_{d=0:D}$ represents the unknown HRF shape in parcel $\mathcal{P}$. Note also that $\boldsymbol{P}\ell_j$ models a low-frequency trend to account for physiological artifacts; we will note $\boldsymbol{l} = (\boldsymbol{\ell}_j)_{j=1:J}$. Variable $\boldsymbol{b}_j$ stands for the noise and for simplicity reasons, we only consider a Gaussian white noise model $\boldsymbol{b}_j \sim \mathcal{N}(0, \sigma^2_{\boldsymbol{b}_j})$. See Fig. 1 for an illustration of this forward modeling.

Within the Bayesian framework, priors are expressed on every sought object: Gaussian prior on $\boldsymbol{h}$ with a smooth constraint on its second derivative expressed within its covariance matrix, spatial mixture models on $\mathbb{a}$, Gaussian non-informative prior on $\boldsymbol{l}$ and non-informative priors on every hyper-parameters $\boldsymbol{\Theta}$. Refer to [1] for their detailed expressions. Assuming no further prior dependence between parameters, formal application of the chain rule yields the expression of the joint posterior distribution $p(\boldsymbol{h}, \mathbb{a}, \mathbb{q}, \boldsymbol{\Theta} \,|\, \mathbb{y})$ ($\boldsymbol{l}$ are analytically marginalized). We indirectly generate samples drawn from this posterior distribution through Gibbs Sampling, for which the full conditional probability density function of each variable needs to be derived. Posterior mean (PM) estimates are computed from these samples according to: $\widehat{x}^{\text{PM}} = \sum_{k=L_0}^{L_1} x^{(k)}/L, \quad \forall\, x \in \{\boldsymbol{h}, \mathbb{a}, \boldsymbol{\Theta}\}$, where $L = L_1 - L_0 + 1$ and L_0 stands for the length of the burn-in period. Note that this estimation process has to be repeated independently over each parcel of a subject's brain.

The main assets of this approach compared to the classical GLM analysis lie in its ability to process *unsmoothed* fMRI data and in the non-parametric HRF modeling. The latter allows the treatment of data with "atypical" dynamics (*e.g.* [6]) and also the detailed study of the HRF shape across regions. The procedure implies an increased computation time compared to a simpler classical GLM approach but is still quite feasible since a whole brain analysis takes around 1.5 hour on a 2.4 Ghz single processor unit.

4. SENSITIVITY ANALYSIS

In the present sensitivity analysis (SA) framework, the outputs of interest are the NRLs $\mathbb{a}$ and HRF $\boldsymbol{h}$ estimates, and the input of interest is the parcellation ($\boldsymbol{\mathcal{P}}$). Considering any one-factor SA methodology [7], the evaluation of $\frac{\partial \mathbb{a}}{\partial \boldsymbol{\mathcal{P}}}$ and $\frac{\partial \boldsymbol{h}}{\partial \boldsymbol{\mathcal{P}}}$ would have to be computed. However, the lack of a closed form expression makes the evaluation of the partial derivative with respect to $\boldsymbol{\mathcal{P}}$ unreachable. Instead, we rather resort to a Monte Carlo scheme where variability in the output is studied when the model is applied to random inputs.

Random parcellations must be generated under reasonable constraints: (i) parcel geometry must be compact and convex to prevent over-streched regions and (ii) parcel size must not be too variable since we rather want to test the effect of position here. Voronoi diagrams satisfy these constraints and are therefore built to generate suitable parcellations.

5. DATA PROCESSING

Real fMRI data were recorded during an experiment designed to map auditive and visual brain functions, which consisted of a single session of $N = 125$ scans lasting $TR = 2.4$ s, each yielding a 3-D volume composed of $64 \times 64 \times 32$ voxels. The paradigm was fast event-related comprising sixty auditive and visual stimuli. An antomo-funtional mask was extracted from these data. It defined the set of positions involved in the generation of parcellations. We considered only the left hemisphere of the brain (half of the original mask) to reduce the problem dimension but still keep regions involved in the paradigm (temporal and occipital area for auditive and visual conditions respectively).

Within this mask, we generated spatially randomized seeds for the Voronoi diagram. Note that peripheral positions were discarded to avoid too small regions. The Voronoi diagram was computed and each voxel labeled using the index of the closest Voronoi patch. Such a parcellation is illustrated in Fig 2(a). We finally produced a set of $\Gamma = 100$ parcellations

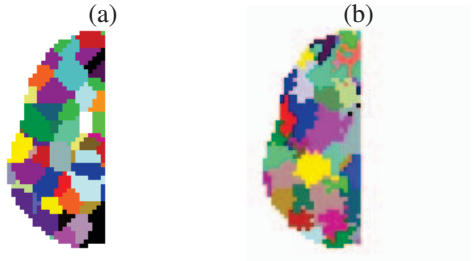

Fig. 2. Parcellations of the brain: (a) using the Voronoi based method - (b) as obtained with an optimal anatomo-functional parcellation as in [2].

denoted $\{\boldsymbol{\mathcal{P}}^{\gamma}\}_{\gamma=1:\Gamma}$. We used each element of this set as input to the JDE procedure applied to the unsmoothed fMRI data.

6. ANALYSIS

For the sake of conciseness, we will only present results concerning the auditive condition ($m = 1$). For each voxel j, we define the set of NRL estimates $\widehat{\boldsymbol{\xi}}_j = \{(\widehat{a}_j)^{\gamma}\}$, and the set of HRF estimates $\widehat{\boldsymbol{\zeta}}_j = \{(\widehat{\boldsymbol{h}}_j)^{\gamma}\}$, with $\gamma = 1:\Gamma$. Note that the JDE procedure yields only one HRF estimate per region. Therefore, to enable multiple comparison of voxels, we assign the regional HRF estimate to every voxel comprising it.

In order to measure the estimation variability induced by varying parcellation, we are interested in the mean NRL estimates and their associated standard deviation, say: $\mathrm{E}[\widehat{\boldsymbol{\xi}}_j]$ and $\sqrt{V[\widehat{\boldsymbol{\xi}}_j]}$. To sum-up the variability of HRF estimations at the voxel level, we will focus on its temporal variability through the standard deviation of its time-to-peak, *i.e* $\sqrt{V[\widehat{\boldsymbol{\tau}}_{ttp}]}$ where $\widehat{\boldsymbol{\tau}}_{ttp} = \{\Delta t \times \mathrm{argmax}_d(\widehat{\boldsymbol{h}}_j)^{\gamma}\}_{j=1:J,\gamma=1:\Gamma}$.

7. RESULTS

Note that all figures concerning the NRL estimates have the same color scale to make comparisons easier.

By way of comparison, Fig. 3 presents results on single runs of the JDE procedure either using an optimal parcellation or a randomized parcellation. A first comparison indicates that the optimal parcellation yields more contrasted NRLs and more clear-cut activation clusters.

In what follows, we consider results of the Monte Carlo sensitivity analysis, *i.e.* results from the JDE procedure iterated over the complete set of parcellations. Fig. 4 depicts results when the parcellation is varied randomly. More precisely, Fig. 4(top row) reports the mean NRL estimations over the Monte Carlo simulations while Fig. 4(bottom row) show their standard deviations. We can first observe that the overall NRLs estimates have comparable values to their standard

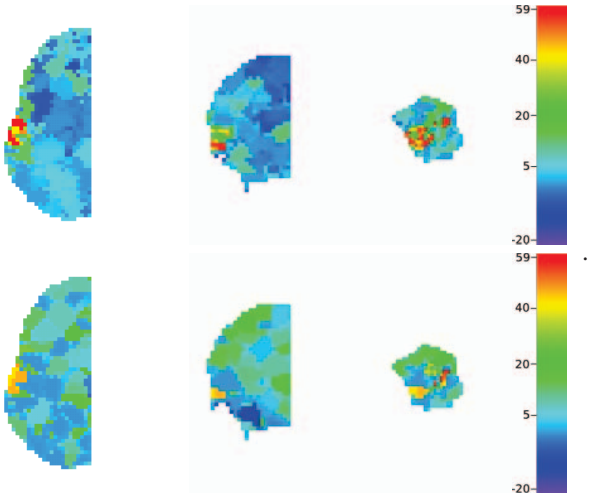

Fig. 3. NRL estimates ($\widehat{\boldsymbol{a}}^1$) as obtained by a single run of the JDE procedure: (top row) using a suitable parcellation as in Fig 2(b) — (bottom row) using a random parcellation as in Fig 2(a). From left to right: axial, coronal and sagittal views.

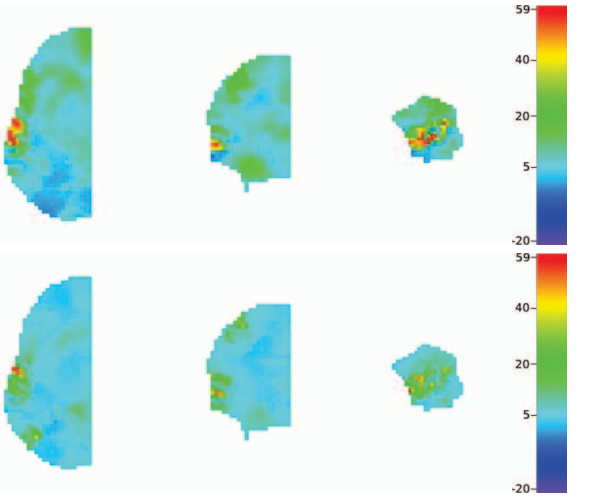

Fig. 4. Results on NRLs when randomizing parcellation: (top row) means of NRL estimates $\mathrm{E}[\widehat{\boldsymbol{\xi}}_j]$ — (bottom row) standard deviation of NRL estimates $\sqrt{V[\widehat{\boldsymbol{\xi}}_j]}$.From left to right: axial, coronal and sagittal views.

deviations, meaning that incertainty on the effect is correlated to its size. It indicates that the JDE is quite sensitive to the input parcellation. Besides, on Fig. 4(top left) we can identify two close activation clusters. As shown in the sagittal view of Fig. 4(bottom row), the more frontal cluster has a strong standard deviation whereas the more occipital cluster shows little standard deviation.

By comparing results in Fig. 4(top row) to Fig. 3(top row), there is a consistency between the mean NRL estimates obtained from multiple JDE runs with Monte Carlo simulations and the NRL estimates obtained with a single JDE run with the optimal parcellation. Nevertheless, this is at the price of

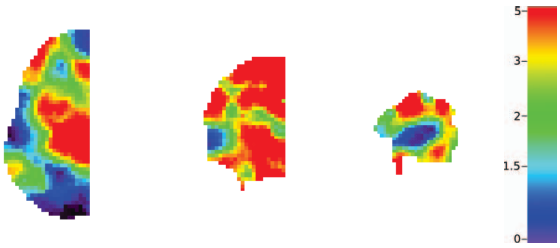

Fig. 5. Results on HRF estimation sensitivity: standard deviations of times-to-peak in seconds. From left to right: axial, coronal and sagittal views.

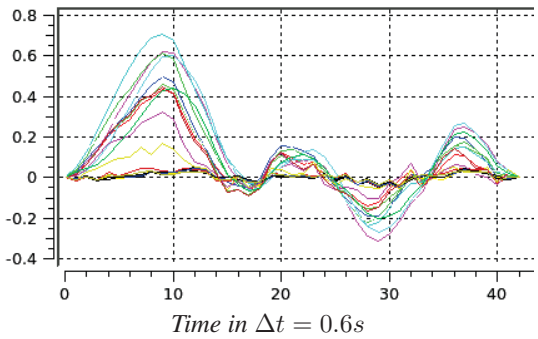

Fig. 6. Results on estimated HRFs at a voxel within an activating cluster, with runs of JDE over different Voronoi-based parcellations. HRFs are color coded corresponding to different runs.

increasing the incertainty.

Results concerning the HRF estimation sensitivity are shown in Fig. 5-6. Time-to-peak maps indicate a good reliability of the dynamics estimation w.r.t. parcellation as standard deviation is around 0.2 s in activating clusters. Note that non-activating regions yield high variability in the HRF estimation, which is sensible since the model tries to fit signals made mostly of noise. Results on the estimated HRF time courses confirm this since the shapes do not vary much w.r.t. parcellation - Fig. 6. Note that scales of HRFs are arbitrary here; they are not relevant since we focus on the *shape* variability.

8. DISCUSSION

In conclusion, since we observe that size of the mean NRL estimates across Monte Carlo simulations are correlated with their standard deviations, we can conclude that the parcel position play an important role in the optimal parcellation and that the local aspect not only prevails in the detection part of the procedure. In contrast, the estimation part of the procedure seems to be less sensitive to the parcellation since estimated HRF shapes vary littlely in activating regions.
Besides, the protocol used here to assess the sensitivity towards position variabililty in the input parcellation of JDE can be seen as a marginalization of this input parameter. Errors associated to each activation cluster then inform on its reliability. For example, we identified one activating cluster associated with strong standard deviation of the NRLs estimates w.r.t parcellation, whereas another cluster was associated to a lower standard deviation. However, coupling the sensitivity analysis to the JDE process is not tenable in terms of computation time (around 10 hours, parallelizing over 30 processors). Therefore, we demonstrate the need for a reliable parcellation prior to the procedure. In another respect, if such parcellation is not achievable, the clustering procedure should be combined with the JDE procedure in an iterative scheme. Formally, this issue takes place in model selection problems and could be addressed for instance using reversible jumps Markov Chain Monte Carlo methods [8].

9. REFERENCES

[1] T. Vincent, P. Ciuciu, and J. Idier, "Spatial mixture modelling for the joint detection-estimation of brain activity in fMRI," in *32th Proc. IEEE ICASSP*, Honolulu, Hawaii, April 2007, vol. I, pp. 325–328.

[2] B. Thirion, G. Flandin, P. Pinel, A. Roche, P. Ciuciu, and J.-B. Poline, "Dealing with the shortcomings of spatial normalization: Multi-subject parcellation of fMRI datasets," *Hum. Brain Mapp.*, vol. 27, no. 8, pp. 678–693, August 2006.

[3] B. Thyreau, B. Thirion, G. Flandin, and J.-B. Poline, "Anatomo-functional description of the brain: a probabilistic approach," in *Proc. 31th Proc. IEEE ICASSP*, Toulouse, France, May 2006, vol. V, pp. 1109–1112.

[4] R. S. Desikan, et al. "An automated labeling system for subdividing the human cerebral cortex on mri scans into gyral based regions of interest.," *Neuroimage*, vol. 31, no. 3, pp. 968–980, July 2006.

[5] S. Makni, P. Ciuciu, J. Idier, and J.-B. Poline, "Joint detection-estimation of brain activity in functional MRI: a multichannel deconvolution solution," *IEEE Trans. Signal Processing*, vol. 53, no. 9, pp. 3488–3502, September 2005.

[6] Maria Gabriella Tana, Anna Maria Bianchi, Paolo Vitali, Flavio Villani, and Sergio Cerruti, "The haemodynamic response to interictal epileptic spikes," in *Proc. of the 29th IEEE EMBS Annual international conference*, Lyon, , France, August 2007, pp. 5223–5226.

[7] Eric Walter and Luc Pronzato, *Identification of Parametric Models from Experimental Data*, Communications and Control Engineering. Springer-Verlag, Berlin, 1997.

[8] Sylvia Richardson and Peter J. Green, "On Bayesian analysis of mixtures with an unknown number of components (with discussion)," *J. R. Statist. Soc. B*, vol. 59, no. 4, pp. 731–792, 1997.